RC 21702 (Log 97765) 03/22/2000
Physical Science

IBM Research Report

Structural and Electronic Characterization of a Dissociated 60° Dislocation in GeSi

P.E. Batson
IBM Research Division
Thomas J. Watson Research Center
PO Box 218
Yorktown Heights, NY 10598

IBM Research Division
Almaden - Austin - Beijing - Haifa - T.J. Watson - Tokyo - Zurich

Structural and Electronic Characterization of a Dissociated 60° Dislocation in GeSi

P.E. Batson
IBM Research, Yorktown Heights, NY 10598, USA

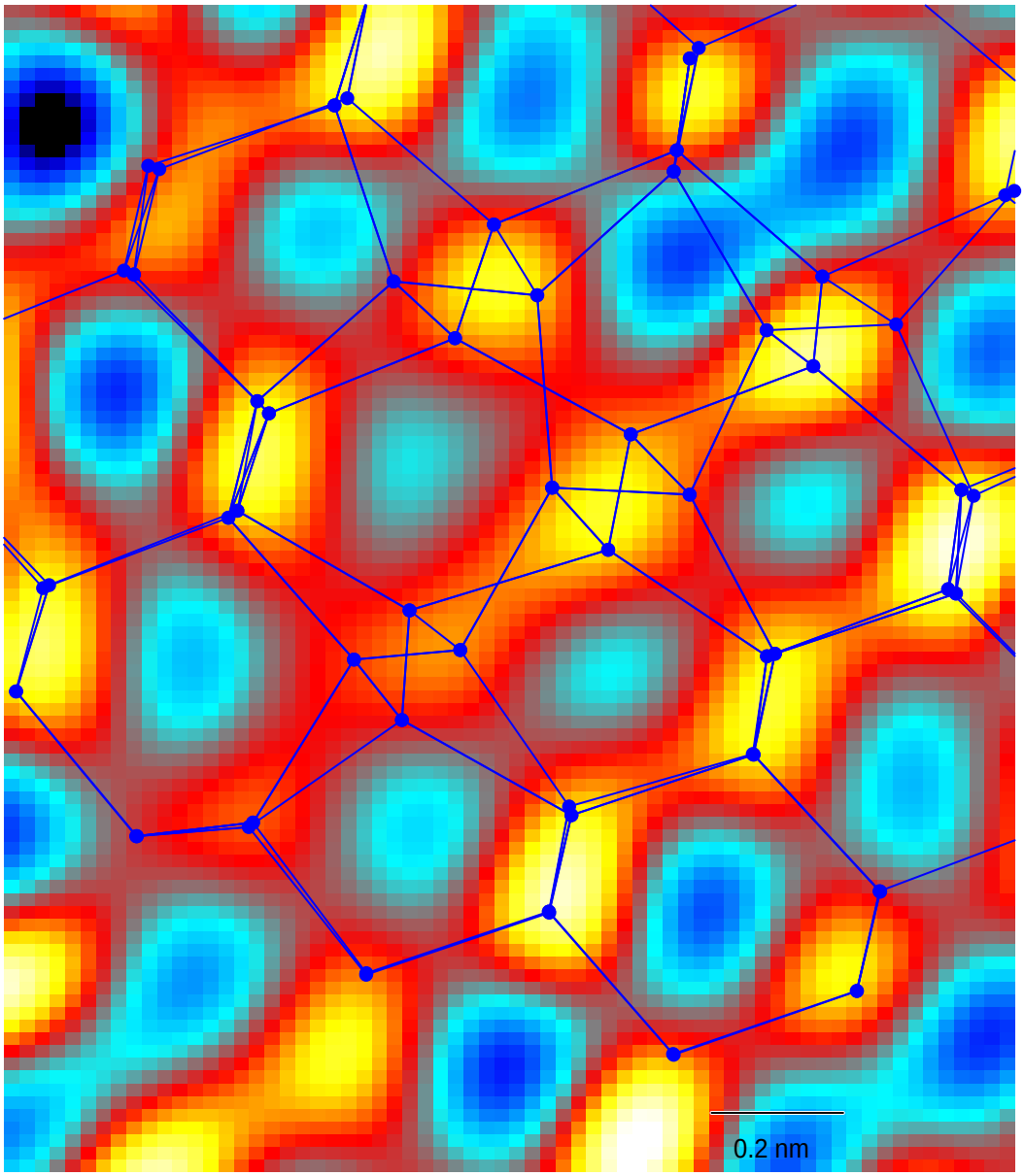

Phys. Rev. B, in press, March 22, 2000

Structural and Electronic Characterization of a Dissociated 60° Dislocation in GeSi

P.E. Batson
IBM Thomas J. Watson Research Center,
Yorktown Heights, NY 10598, USA

Abstract

A dissociated 60° misfit dislocation at the substrate interface of a $Si/Ge_xSi_{(1-x)}$ heterojunction has been examined using EELS and ADF imaging. New spectra are obtained at the intrinsic stacking fault, at the dislocation cores and in the strained regions on either side of the stacking fault. In gap states are verified at the partial dislocation cores. Images resemble accepted structures except at the 90° partial dislocation. Model structures for the object are considered to try to reconcile the imaging and spectral results.

I. INTRODUCTION

It is well known that when the thickness of a thin film exceeds the Matthews-Blakeslee value for pseudo-morphic growth, misfit dislocations are introduced at the underlying heterojunction. [1] In the case for Si growth on the [0 0 1] surface of $Ge_xSi_{(1-x)}$, the misfit takes the form of a 60° dislocation dissociated into 30° (P30) and 90° (P90) partial dislocations separated by an intrinsic stacking fault (ISF). This structure has been suspected to contribute to limited electron mobility in strained $Si/Ge_xSi_{(1-x)}$ hetero-structures. [2]

These structures also occur in heavily deformed silicon, and are believed to support electrically active states within 0.1 eV of the conduction band (CB) minimum. [3,4] TEM and luminescence studies have confirmed optical activity near the defect, but the atomic structure that gives rise to the activity is not yet known. [5–9] Optical activity has also been detected associated with misfit structures. [10]

Theoretical work with likely core structures has not found strong evidence for optical activity at either the stacking fault, [11–13] or at straight partial dislocations bounding the fault, [14–16] largely because it was found that the dislocation cores reconstruct to clear the gap of electronic states. Recent studies of 90° core structures also find that they are likely to reconstruct to lower their total energy. [17,18] Finally, there has been some theoretical evidence for shallow valence band states. [19]

I report here experiments using spatially resolved Electron Energy Loss Spectroscopy (EELS) to probe small regions of dissociated misfit dislocations in a strained Si quantum well imbedded in $Ge_{0.35}Si_{0.65}$. [20] The results reveal the local CB at the 30° dislocation (P30), the intrinsic stacking fault (ISF), and the 90° dislocation (P90), and in the strained regions nearby the defect. Atomic column positions in the [1 1 0] projection, and the spatial location for the spectral results

are obtained using Annular Dark Field (ADF) imaging in the Scanning Transmission Electron Microscope (STEM).

II. EXPERIMENTAL DETAILS AND DESCRIPTION OF THE DISLOCATION

These studies have used the VG Microscopes STEM, heavily modified to operate at 120 KV to obtain a 0.2nm diameter electron probe. Using this probe size, atomic columns can be resolved in the Si and GeSi alloys using ADF imaging in the [1 1 0] projection. [21,22] In prior work with GeSi alloys and strained Si channels, it has been shown that very detailed Conduction Band (CB) information is obtainable using high resolution, spatially resolved EELS measurements of the Si $2p_{3/2}$ core absorption edge. [23–26] The EELS spectrometer was a Wien Filter design with an energy resolution of ∼200 meV and an absolute calibration of ±20 meV. [27,28] Since the field emission source in this instrument has a natural energy spread of about 0.3 eV, the spectral resolution after numerical deconvolution was limited to 0.20-0.25 eV by statistical considerations. [29] The most important experimental limitation was the mechanical specimen drift of ∼ 0.1nm/min. In the past, measurements have been restricted to 1-2eV resolution to shorten the measurement time, or have been obtained from regions scanned parallel to a boundary to minimize this problem. This work combines both the high resolution EELS information with a very high position accuracy of better than 0.1-0.2nm.

The misfit dislocation was of the 60° type located at the substrate interface of a 15nm Si quantum well structure. This structure was deliberately grown to exceed the critical thickness for misfit dislocation nucleation to investigate the effect of dislocation presence on electron mobility. [2] Fig. 1 shows a low magnification bright field image of a cross section of the structure. The Si well (bright band) lies on the right. The misfit dislocation investigated in this work is indicated by the arrow. Notice that the surface of the sample, on the right, is not smooth, but has facets with boundaries near the dislocation. These facets are highlighted by dashed lines in the figure. There are also many complex dislocation structures buried deeply in the substrate. This work addresses only the simplest structure which lies immediately under the strained well.

Fig. 2 shows an Annular Dark Field (ADF) and Bright Field (BF) image pair of the [1 -1 0] projection of the structure at high magnification. The images have been rotated to place the Si well at the top, above the dashed line. The dislocation is extended about 2nm in the [1 1 -2] direction away from the Si interface. The high angle ADF image (a) provides an atom column image with column brightness that reflects the amount of Ge within the column. Since the inter-column distance in the [0 0 1] direction in this projection is about 0.135nm, this distance is not resolved in this image. Instead, for each pair of columns, we see one spot, elongated in the [0 0 1] direction. As can be seen in the image, the position of the ISF can be found by noticing where the elongated spot rotates from the [0 0 1] direction to a [2 2 1] direction, lying nearly parallel to the Si interface. As we shall see below, the P30 dislocation lies within or nearby the Si interface. The P90 dislocation lies at the other end of the ISF. The BF image (b) shows lattice periodicities, but does not show atom positions because the resolution in this mode of imaging is about 0.28nm. The bright spots in this image are as likely to be holes as atom columns. Neither does it give any indication of the location of the Ge/Si interface, because the small angle scattering which gives this image is not sensitive to atomic number. On the other hand, this image is very sensitive to strain, showing regions of large strain (dark regions) at either end of the ISF. Notice that the strained region near the P30 dislocation is pushed into the GeSi substrate. It is known that the alloy is

softer than Si, so this is an expected result.

Fig. 3 shows a higher magnification ADF image after applying a 0.15nm smoothing filter to reduce measurement noise, reproduced from [20]. The image is a [1 -1 0] projection of the [0 0 1] substrate/well interface (dashed line). The measured distance between the two partial dislocations is 3.3 nm, or 10 "dumbbell" units. This distance was found in other simple misfit structures elsewhere in this sample. The P30 core is well defined, but the P90 core appears indistinct, probably due to kinks occurring along its length. [6,30] However, it can be located by considering continuity of [1 1 -1] type atomic planes as they cross the ISF. Inspection of the P30 core reveals a very close agreement with the glide-cut structure, [15] but the P90 core image does not readily agree with the simple 5-7 fold ring structure. [31] This is perhaps not surprising given that many kinks are expected to be present. This Figure defines several unique locations for EELS analysis: a) the bulk, relaxed GeSi alloy several tens of nm away from the defect, b) the regions of tension and c) compression within two [1 1 1] plane spacings on either side of the ISF, d) the ISF itself, e) the P30 dislocation core and f) the P90 core.

III. EXPERIMENTAL RESULTS

Si 2p core absorption spectra are processed to remove a slowly varying background, to sharpen the energy resolution by deconvolution of the incident beam energy distribution, and to remove the $2p_{1/2} \rightarrow$CB intensity. The shape of the remaining intensity is due to transitions to the s- and d-projected CB Local Density of States (LDOS). A model spectrum is generated from a trial LDOS, using an inelastic scattering theory including core excitonic interactions, lifetime broadening and instrumental resolution. The model LDOS consists of parabolic effective mass contributions for the s-like band edges at Δ_1, L_1, and a saddle point at the d-like point L_3. These contributions are terminated linearly at the p-like points $\Gamma_{1,5}$ and $\Gamma_{2'}$ in the center of the Brillouin Zone. The model positions for the important band edges Δ_1 and L_1 are then adjusted to fit the experimental data. This method allows a determination of CB offsets in the GeSi alloy series with an accuracy of $\pm$20 meV. [23] Finally, there is a small contribution to the L_1 intensity due to a Ge-like saddle point in the Λ_1 band.

In Fig. 4 there are spectral results for each of the regions described above. Each spectrum includes the processed data, a trial LDOS and the fitted spectrum. The spectra are aligned on an absolute energy scale relative to the $2p_{3/2}$ core level. This level has been shown to be a constant for the relaxed alloy series. [24] But it is assumed to shift with the addition of crystal strain. [32]

A. Bulk Relaxed and Strained Alloy Areas

The bulk alloy results in Fig. 4 match the prior results closely for the alloy composition $Ge_{35}Si_{65}$. [23] This value was confirmed by x-ray scattering lattice measurements. The four usual CB features, Δ_1, L_1, L_3, and Λ_1, are required to fully explain the measured data. In the regions of tension and compression, the most notable change is to shift the spectra lower or higher in energy. A secondary difference is an apparent broadening of the L_1 contribution in the compressed region. In order to understand these results, we need to consider two kinds of effects. First, volume strain shifts both the core level and the CB levels, but the sign of the shift depends on the symmetry of the electron states. For instance, bonding orbitals shift downwards in energy for negative strain:

they become more energetically favorable at smaller inter-atomic distances. The Δ_1 CB of Si and the SiGe alloys also has bonding character and therefore also shifts to lower energies when the lattice constant is made smaller. [24] The L_1 CB, on the other hand, shifts upwards with smaller lattice constant, more in keeping with the behavior of anti-bonding symmetry. The second effect of strain is to change the shape of each band contribution for non-isotropic strains. An example of this is the bi-axial strain splitting of the Δ_1 CB within the strained Si well where a two-fold piece of Δ_1 shifts downwards, forming the high mobility conduction channel, while the lower mobility four-fold piece shifts upwards.

In the present case, we expect volume strain and uniaxial strain in the [1 1 1] type directions. The experimental data show a Δ_1 shift of -0.085eV for the region in tension and +0.10eV in compression. These shifts are opposite those expected for the CB involved and so we expect a large core level shift. Within a couple [1 1 1] lattice planes on either side of the ISF, inspection of the image shows that this 10 unit ISF has 10 atomic planes on one side and 11 planes on the other, occupying roughly 10.5 bulk lattice units, giving a lattice strain of $\pm 5\%$ on either side. The deformation potential for the Si $2p_{3/2}$ core level is about -6 eV [32] giving a core level shift of -0.3 eV at 5% tension and +0.3 eV in compression. Therefore these measurements place the Δ_1 CB at +0.22 eV at b) in tension, and -0.20 eV at c) in compression, relative to the bulk alloy. The band offset in the Si well in this case is about -0.28 eV so this is a significant perturbation of a desired device quantity. The deformation potential for Δ_1 is +4 eV, [32] and therefore provides a satisfying consistency to the interpretation.

These areas should also be subject to a uniaxial strain of [1 1 1] type symmetry. These are somewhat more difficult to deal with in that they result in splitting of the 8-fold degenerate L_1 bands into 2-fold/6-fold combinations. Again, inspection of the image suggests that the uniaxial strain is about $\pm 5\%$ within a [1 1 1] plane, but oriented in a [1 1 2] type of direction. The appropriate deformation potential for this process appears to be Ξ_u^L and is 15-16 eV [32]. The shifts are expressed relative to the strain $\epsilon_{xy} = 1/3(\epsilon_\perp - \epsilon_\parallel) \approx 0.1\epsilon_{111}$ for this case. This leads to a shift of the 2-fold part of the band by about 0.15eV and the 6-fold part by 0.05 eV in the opposite direction. An experimental determination of these quantities is made difficult by the disparity in degeneracy, leading to a disparity in measured intensities for the two contributions – it is very difficult to locate the position of the 2-fold part of the scattering with any accuracy. In Fig. 4 the total model splitting for the best fit to the data is indicated by the dotted lines attached to the L_1 point in the bulk results. In the case of Tension, the 2-fold edge falls over the edge of the Δ_1 contribution. Therefore, the spectrum appears to have only one, less intense, L_1 peak. In the compression case, the 2-fold piece shifts upwards in energy, where the underlying Δ_1 contribution is flat, leading to an apparent broadening of the L_1 peak. This modeling arrives at a total splitting of 0.26 eV, compared with 0.20 eV expected from the deformation potential.

B. Intrinsic Stacking Fault

Spectral results from position d), the ISF show a splitting of the L_1 peak, with no other apparent shifts or changes. In particular, there appears to be no shift or change in shape of the onset at Δ_1. The splitting can be understood using the calculations for Si of Mattheiss and Patel. [12] They predicted that the L_1 branch is affected in two ways. First, it is projected into the center of the 2-D hexagonal ISF Brillouin Zone (BZ) by the two dimensional nature of the fault. Then it is split into two components by mixing of Si sp^3 orbitals from third-neighbor atoms on either

side of the glide-cut plane. An atomic model of a P90 partial dislocation is reproduced in Fig. 5 to illustrate this structural change. In the parent crystal, third neighbor atoms occupy positions on either end of a structure commonly referred to as a "chair". In the ISF structure, as a consequence of the 180° rotation of the structure about the [1 1 1] direction, the third neighbors form a "boat" structure, moving from their normal 0.45nm distance apart to nearly the second neighbor distance of 0.38 nm.

I model the band splitting that results from this by introducing a gap in the L_1 band, labeling the upper and lower branches, Γ^+ and Γ^-, following the notion that the band is projected into the 2-D zone center and split into symmetric and anti-symmetric parts by the 3rd neighbor interaction. This splitting is calculated to be about 1.5 eV for Si, while the lower band is calculated to shift about 0.25 eV down from the L_1 minimum in the bulk. These predictions strongly resemble the observed behavior. The work also predicts that the X_1 CB in the bulk lattice, for which Δ_1 is the band minimum, becomes the Γ-M band in the hexagonal ISF BZ and is not affected by the change in local symmetry at the ISF. Again this is reflected in the data of Fig. 4, which shows no change at the ISF Δ_1 onset relative to the bulk alloy.

This experimental result argues against the presence of in-gap empty states near the CB. It obviously does not address the possibility of states near the valence band edge, although it indirectly supports the possibility of their presence because they are predicted within the Mathiess and Patel work, which appears consistent with these results in areas where it can be checked.

C. P30 Dislocation Core

Fig. 6 shows a cut from the experimental image compared with the reconstructed glide plane terminated core model from Chelikowsky. [15] Agreement is quite good except near the Si well, where Fig. 1 clearly showed a non-ideal strain contrast.

Spectral results in Fig. 4 for the P30 dislocation show splitting of the L_1 peak that is almost identical to that seen at the ISF. Yet reference to the model structure reproduced in Fig. 7 does not readily show "boat" structures that characterized the appearance of L_1 splitting in the discussion above. However, further consideration reveals that not only are the 3rd neighbor distances changed at the ISF, but the local D^4_{6h} symmetry, characteristic of the bulk crystal, is broken by the ISF rotation to produce a D^3_{3d} local symmetry. Fig. 8 shows comparisons between local structural units to illustrate this behavior, In the case of the bulk structure, a screw axis, lying between near neighbors, transforms the upper 2nd neighbor positions into the lower positions. In the ISF structure, a mirror plane does a similar operation. The existence of the mirror plane is what splits the L_1 band. Returning now to Fig. 7, we see that the ISF does indeed show a structure containing the mirror symmetry. But surprisingly, the P30 does as well, although it is oriented in a [1 1 0] type direction rather than in a [1 1 1] direction. It can be concluded that the reconstructed core P30 is consistent with the finding of splitting in the L_1 band at the dislocation core. It will be shown below that this visual analysis can be put on a more sound statistical basis.

D. P90 Dislocation Core

Fig. 9 shows a comparison of the Single Period (SP90) reconstructed P90 structure with the recorded data. This consists of 5-7 fold rings joined across the core. Agreement appears good

except for the shapes of the spots in the image. Referring to the numbered columns, it can be seen that columns 1-2 and 5-10 are clearly elongated in the expected directions. Columns 3 and 4 are obviously round. While columns 11 and 12 appear slightly elongated but do not point in the expected directions.

What do the spectral results indicate? In Fig. 4, the P90 results are clearly bulk-like. They do not show any splitting of the L_1 intensity. On the other hand, Fig. 5 above, which shows the atomic structure of the single period reconstruction, clearly shows that the atoms on either side of the dislocation (labeled a) lie in "boat" configurations relative to each other. It would seem that this structure may not be consistent with the spectral results.

An new model for the P90 has recently been suggested by Bennetto, Nunes and Vanderbilt. [17,18]. This introduces a Double Period (DP90) reconstruction at the core through the addition of kinks in the plane of the ISF. Viewed in the [1 1 1] direction, these have the effect of creating 5-7 fold rings along the dislocation core. Views in various directions are shown in Fig. 10 for the "qudn" variant of their model. This model has the interesting property that, if viewed in the [1 1 0] direction at 0.2nm spatial resolution, the four core atoms would not be resolved, instead appearing as a single azimuthally symmetric blob. As should in Fig. 11, this provides better agreement with the measured image intensities. In addition, a careful counting of 3rd neighbors and their positions suggests that the ISF-like behavior that gives rise to the splitting of the L_1 is reduced for this model. Improved agreement with the image data can be found if this structural reconstruction is continued to three neighboring double column positions. Fig. 12, shows a structure for an Extended Double Period (EDP90) reconstruction. In this case, 4-8 fold ring structures are introduced at the core. The P90 core takes on a much more extended, quasi-random nature. A better match with the imaging data, as shown in Fig. 13, is the result. As will be discussed in more detail below, however, this structure may not be energetically favored over the DP model.

IV. STATISTICAL ANALYSIS OF A LARGE MODEL STRUCTURE

The discussion above depends critically on the local behavior of the 3rd neighbors within a very narrow region of highly distorted crystal. Therefore there needs to be a method for evaluating this behavior in a quantitative way. This requires, firstly, that we have a realistic model atomic structure for the entire P30-ISF-P90 dislocation complex. In Fig. 14 is displayed a 200 atom cut from an 810 atom model of the entire structure for the case of the Single Period reconstructed P90 core. The model consists of four (1 -1 0) single atom layers extending far enough away from the complex that local strain at the edges is small. At the dislocation cores, I have used calculated structures from several sources (P30 [15], P90 [16,17]). After insertion of the published core structures into the large model, the structures were adjusted by hand to reproduce the Si-Ge bond length to within $\pm 8\%$. Finally, they were relaxed by Y. Tu using a Keating potential with fixed boundaries in the [1 -1 0] plane, chosen to match the imaging data, and periodic boundary conditions perpendicular to this plane. A deficiency in this particular model is that no attempt was made to reproduce the change in elastic coefficients, on going from the GeSi alloy to the Si well, that were present in the original. For the purposes of this study, we assume that all atoms are Si. Clearly, as was pointed out above with Fig. 2, strain near the Si well is influenced by this.

The ISF-like 3rd neighbor symmetry breaking behavior can be quantitatively investigated within this structure by projecting an atom and its neighbors onto each of the possible four (1 1 1) type planes and then characterizing the azimuthal position, ϕ, of the atoms in that projection

with a structure factor (ASF) $e^{i3\phi}$. Summation of these factors for the 3rd neighbors yields 0 for a 6-fold, bulk-like structure and 6 for a 3-fold ISF-like structure. Fig. 15 shows plots of this structure factor against 3rd neighbor distances for each of the structures discussed above – bulk, ISF, P30, SP90, DP90 and EDP90, reproduced from [20]. We find that this technique properly characterizes the bulk and ISF regions. It identifies the P30 as likely having 3-fold symmetry, with an appropriately small 3rd neighbor distance. It fairly strongly indicates that both the SP90 and the DP90 structures have some 3-fold symmetry and therefore likely would support the L_1 splitting. A caveat to this finding is that the 3rd neighbor distances are longer than those found at the ISF and P30, so the expected splitting would be smaller and therefore, perhaps, less easy to identify. Finally, it identifies the EDP90 structure as being the most likely to suppress the ISF-like L_1 behavior.

V. NEAR EDGE INTENSITY AT THE DISLOCATION CORES

Turning to the P30 near edge structure at Δ_1, summarized in Fig. 16, there apparently exist near edge gap states at the dislocation core. For everywhere except near Δ_1, the ISF model fit is a very good match to the data. When this fit is subtracted from the P30 data, a peak remains centered at the Δ_1 onset. It's width is close to the instrumental resolution of 0.2 eV. In addition, excess intensity remains near the L_3 peak. It is known that this peak is symmetry compatible with Δ_1 – that is they have symmetry elements in common – and that they shift together under strain. [23] Therefore, it is reasonable that any distortion in the crystal that gives rise to splitting of states into the gap from Δ_1 should also shift states downwards from L_3.

Fig. 17 shows a similar analysis for the P90 EELS results. In this case the fitted model for the bulk results has been subtracted from the data to reveal that a peak exists about 80 meV below the onset of Δ_1. Also, in this case, a second peak exists near L_3, as it must if the near edge peak is actually due to the splitting of states from the CB edge.

These two results, together with the results from the ISF and strained regions above, suggest that optical activity involving empty states near the CB is likely to be confined to the dislocation cores. Electrical activity may also be associated with the regions of strain on either side of the ISF, since 80meV peaks and valleys in the CB offset are certainly present there.

VI. CONCLUSIONS

This study has attempted to make a detailed examination of the EELS and atomic structure of the dissociated 60° misfit dislocation. Splitting of the L_1 CB structure is almost certainly due to local symmetry breaking by the presence of ISF-like atomic structure. Near edge gap states are found at the partial dislocation cores, leading one to surmise that optical activity exists at these locations. No information about near Valence Band (VB) edge states can be obtained from these results, so the possibility of optical activity near the ISF due to excitations from a shallow VB state remains. Future work on these structures will be undertaken using improved EELS and imaging capabilities that are currently under development.

Model structures in for this work were relaxed by Y. Tu at IBM. I acknowledge also discussion with P.M. Mooney, F.K. LeGoues, and K. Ismail during this work. R.W. Nunes kindly provided atomic coordinates for the DP structure.

REFERENCES

[1] J.W. Matthews and A.E. Blakeslee, J. Crys. Growth **27**, 118 (1974).

[2] K. Ismail, F.K. LeGoues, K.L. Saenger, M. Arafa, J.O. Chu, P.M. Mooney, and B.S. Meyerson, Phys. Rev. Lett. **73**, 3447 (1994).

[3] L.C. Kimerling, H.J. Leamy, and J.R. Patel, Appl. Phys. Lett. **30**, 217 (1977).

[4] J.R. Patel and L.C. Kimerling, J. Phys. Coll., Paris **40**, 67 (1979).

[5] H. Alexander, J. Phys. Coll., Paris **40**, 1 (1979).

[6] A. Olsen and J.C.H. Spence, Phil. Mag. A **43**, 945 (1981).

[7] H. Alexander, J.C.H. Spence, D. Shindo, H. Gottschalk, and N. Long, Phil. Mag. A **53**, 627 (1986).

[8] V. Higgs, E.C. Lightowlers, C.E. Norman, and P. Knightley, Mater. Sci. Forum **83 − 87**, 1309 (1992).

[9] J. Weber, Solid State Phenom. **37 − 38**, 13 (1994).

[10] Kai Shum, P.M. Mooney, and J.O. Chu, Appl. Phys. Lett. **71**, 1074 (1997).

[11] C. Weigel, H. Alexander, and J.W. Corbett, phys. stat. sol. (b) **71**, 701 (1975).

[12] L.F. Matheis and J.R. Patel, Phys. Rev. B **23**, 5384 (1981).

[13] M.Y. Chou, M.L. Cohen, and S.G. Louie, Phys. Rev. B **32**, 7979 (1985).

[14] J.E. Northrup, M.L. Cohen, J.R. Chelikowsky, J. Spence, and A. Olsen, Phys. Rev. B **24**, 4623 (1981).

[15] J.R. Chelikowsky, Phys. Rev. Lett. **49**, 1569 (1982).

[16] J.R. Chelikowsky and J.C.H. Spence, Phys. Rev. B **30**, 694 (1984).

[17] J. Bennetto, R.W. Nunes, and David Vanderbilt, Phys. Rev. Lett. **79**, 245 (1997).

[18] R.W. Nunes, J. Bennetto, and David Vanderbilt, Phys. Rev. B **57**, 10388 (1998).

[19] F. Liu, M. Mosteller, V. Millman, M.F. Chisholm, and T. Kaplan, Phys. Rev. B **51**, 17192 (1995).

[20] P.E. Batson, Phys. Rev. Lett. **83**, 4409 (1999).

[21] S.J. Pennycook and L.A. Boatner, Nature **336**, 565 (1988).

[22] R.F. Loane, E.J. Kirkland, and J. Silcox, Act. Crys. A **44**, 912 (1988).

[23] P.E. Batson and J.F. Morar, Appl. Phys. Lett. **59**, 3285 (1991).

[24] J.F. Morar, P.E. Batson, and J. Tersoff, Phys. Rev. B **47**, 4107 (1993).

[25] P.E. Batson and J.F. Morar, Phys. Rev. Lett. **71**, 609 (1993).

[26] P.E. Batson, Ultramicroscopy **59**, 63 (1995).

[27] P.E. Batson, Rev. Sci. Inst. **57**, 43 (1986).

[28] P.E. Batson, Rev. Sci. Inst. **59**, 1132 (1988).

[29] P.E. Batson, D.W. Johnson, and J.C.H. Spence, Ultramicroscopy **41**, 137 (1992).

[30] Y.M. Huang, J.C.H. Spence, and O.F. Sankey, Phys. Rev. Lett. **74**, 3392 (1995).

[31] P.B. Hirsch, J. Phys. Coll., Paris **40**, 27 (1979).

[32] C.G. Van de Walle, Phys. Rev. B **39**, 1871 (1989).

FIGURES

FIG. 1. Overview of the [1 -1 0] projection for the 30°/ISF/90° structure investigated in this study. The Si well is the lighter band running from top to bottom on the right. Notice that the misfit dislocation appears to have produced faceting of the surface – highlighted by the dashed lines that follow the surface.

FIG. 2. a) ADF image of the [1 -1 0] projection of a 30°/ISF/90° structure at the substrate interface of a strained Si quantum well. The Si quantum well lies above the interface indicated by the dashed line. b) Small angle BF image of the same area as in a). Strain contrast is visible as the dark regions. The BF spatial resolution is poorer than the ADF resolution and atom columns are not uniquely identified.

FIG. 3. ADF image of a second misfit dislocation structure. Detailed EELS results were obtained from this structure.

FIG. 4. Spatially resolved EELS results for the Si 2p→CB absorption edge for various locations within the structure summarized in Fig. 3. Several structural effects modify the relaxed alloy shape, including strain in tension and compression, the ISF and the P30 and P90 cores. There appear to be unoccupied electron states below the CB within the dislocation cores, but not within the ISF.

FIG. 5. The single period P90 dislocation region. This illustrates the relationship between the bulk, "parent" lattice and the faulted ISF structure. In the bulk, "chair" structures characterize a local environment having 0.45nm 3rd neighbor distances. In the ISF, "boat" structures result in 0.38nm 3rd neighbor positions, and break the local symmetry to produce splitting in the L_1 CB minimum.

FIG. 6. Comparison of [1 -1 0] experimental data with the accepted P30 core model. The apparent single column at the dislocation core identifies this as a glide-cut rather a shuffle structure.

FIG. 7. P30 model structure viewed off the [111] direction to reveal the p30 core structure. Notice that there exists a plane of mirror symmetry perpendicular to the [1 -1 0] direction within the reconstructed core. This resembles the local symmetry of the ISF.

FIG. 8. Relationship between the "boat" and "chair" structures to the change in local symmetry caused by the 180° rotation of the lattice about the (111) direction at the ISF. ISF-like or Bulk-like environments can be identified by testing for the presence or absence of the local mirror plane.

FIG. 9. Comparison of single period reconstruction with experimental structure at the P90 dislocation. Double Si columns are revealed as elongated spots. The existence of round spots within the core argues against the single period core structure. This agrees with the finding that ISF-like structures, notably evident in Fig. 8, are strongly present in this structure.

FIG. 10. Summary of the "qudn" variant of the Double Period reconstruction model for the P90 core. The model assumes alternating kinks at the core, producing 5-7 fold ring structures. The structure reduces the number of 3rd neighbors at ISF distances.

FIG. 11. Comparison of double period reconstruction with experimental structure at the P90 dislocation. This structure reproduces the round spot at the core center, but misses the round spot displaced from the core center (arrow). In addition, this structure has some third neighbor interactions that should produce ISF-like behavior in the EELS spectra which is not seen.

FIG. 12. Summary of an extended Double Period reconstruction that completely eliminates the number of 3rd neighbors at ISF positions. It consists of a "qudn" Double Period reconstruction with three neighboring reconstructions having a similar type. The result has 4-8 fold ring structures at the P90 core.

FIG. 13. Comparison of extended core reconstruction with experimental structure at the P90 dislocation. This structure reproduces round spots displaced from the core center. In addition, it eliminates 3rd neighbor interactions, favoring the existence of more bulk like structure in the spectra.

FIG. 14. Part of the model structure used to investigate the local symmetry of various atomic sites within the defect structure. The P90 core is a single period reconstruction in this example. The [1 -1 0] projection is plotted about 6° off the correct axis to reveal the out-of-plane bonding.

FIG. 15. Results of analyses of the 3rd neighbor distances and local symmetry for several positions within the model structure. As described in the text, an azimuthal structure factor identifies the presence or absence of the ISF-like mirror plane which is likely to be associated with the splitting of the L_1 CB.

FIG. 16. EELS analysis for the P30 partial dislocation. The solid line reproduces the fit to the ISF data. There is extra intensity coincident with the CB onset.

FIG. 17. EELS analysis for the P90 partial dislocation. The solid line reproduces the fit to the bulk alloy data. There is extra intensity about 80 meV below the CB onset in this case.

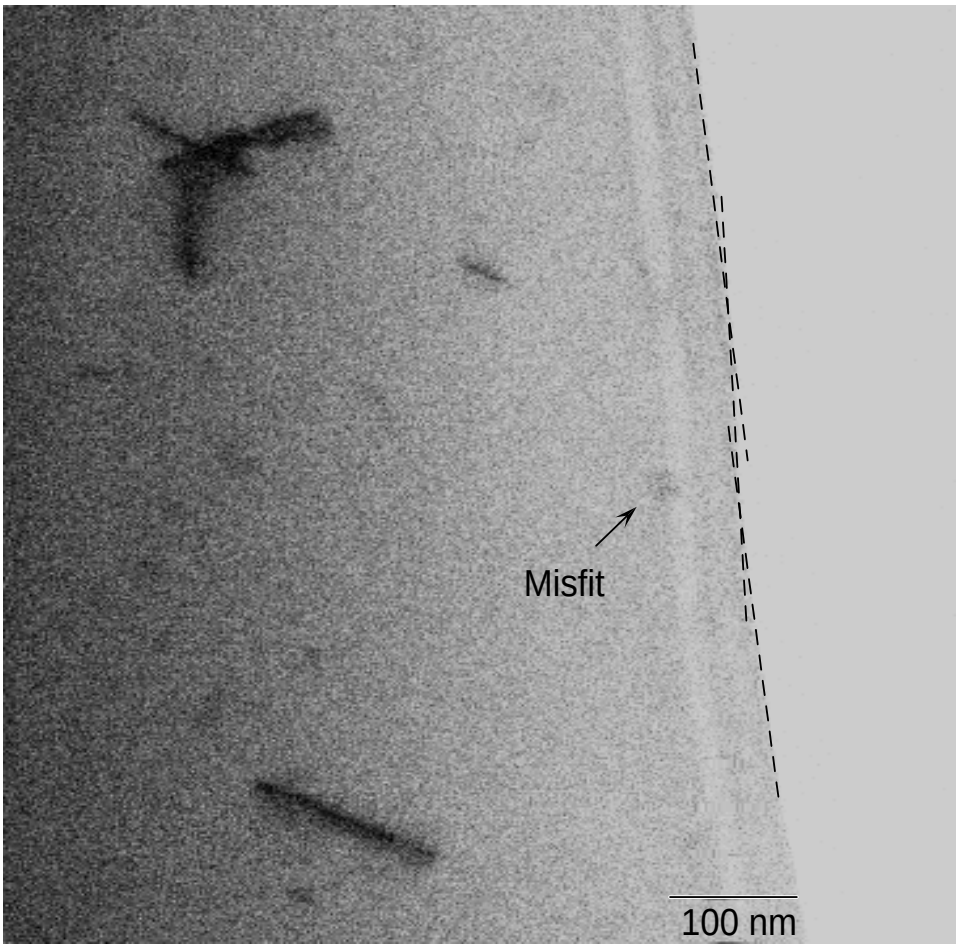

Figure 1

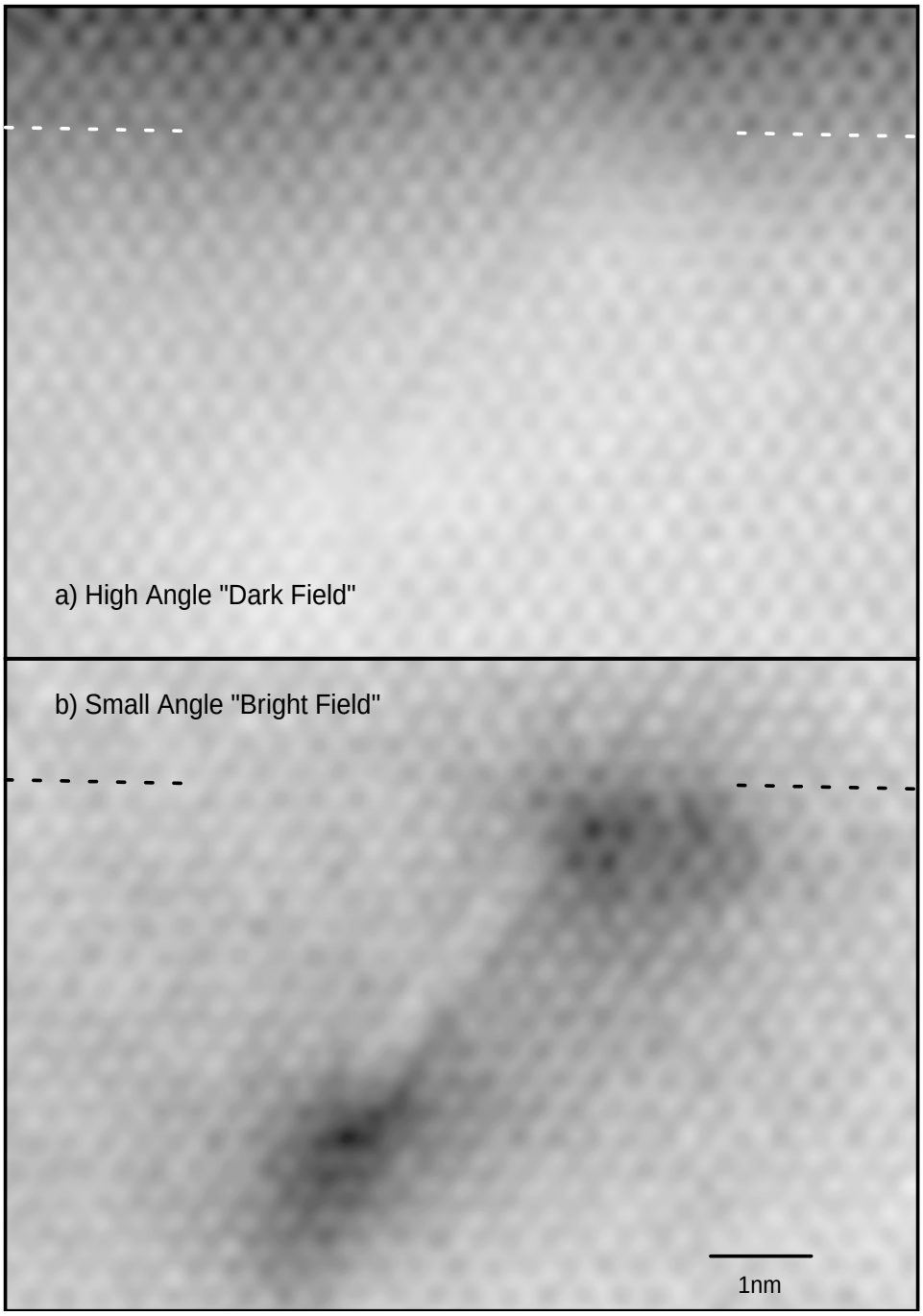

Figure 2

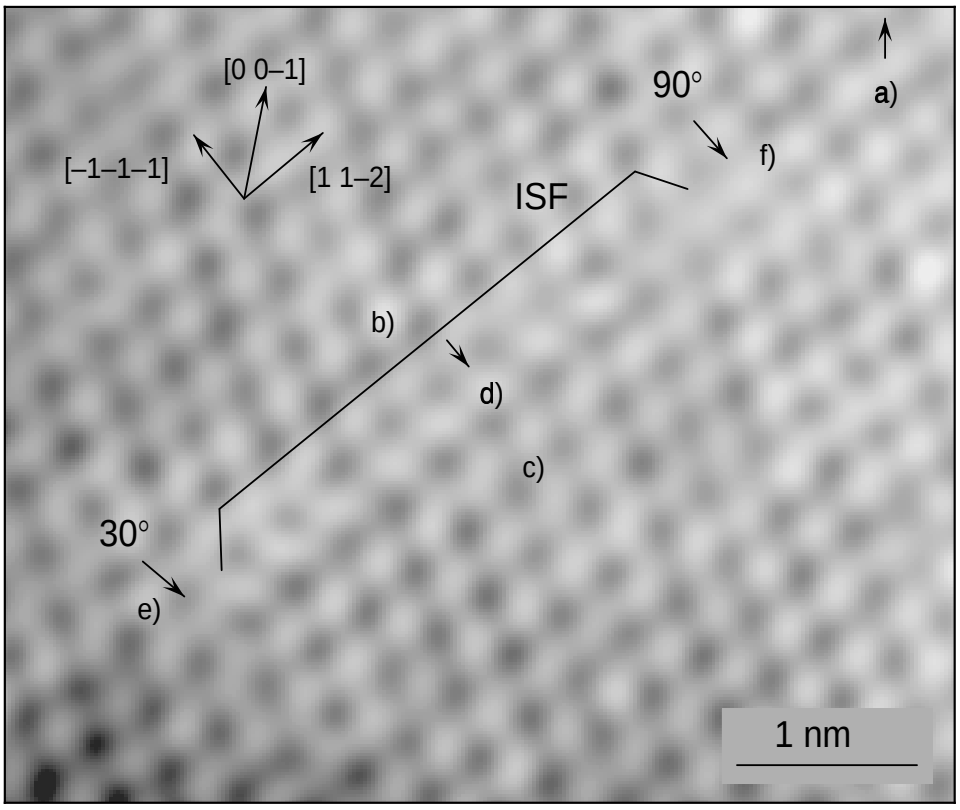

Figure 3

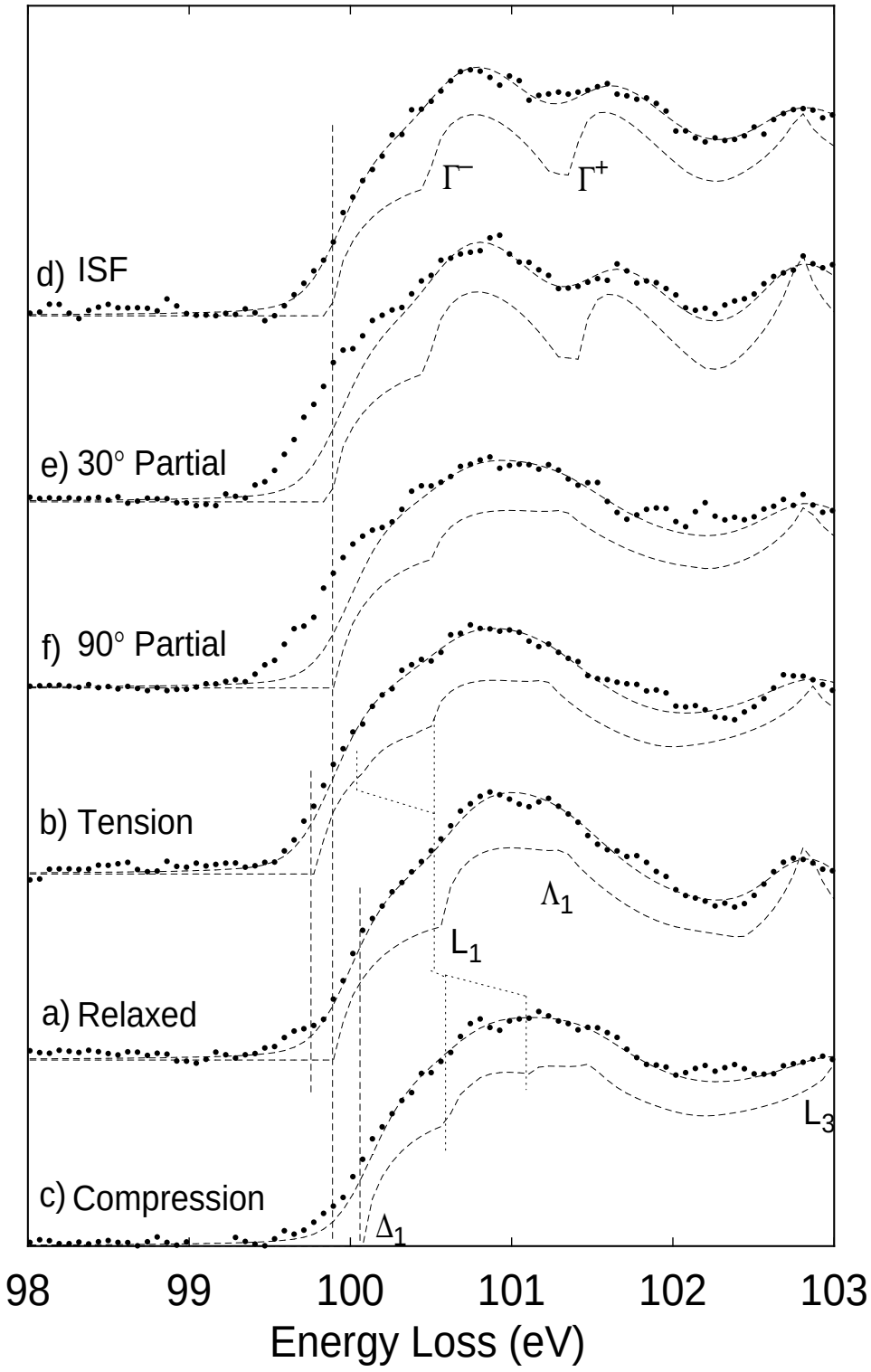
Γ⁻
Γ⁺
d) ISF
e) 30° Partial
f) 90° Partial
b) Tension
Λ1
L1
a) Relaxed
L3
c) Compression
Δ1
98
99
100
101
102
103
Energy Loss (eV)

Figure 4

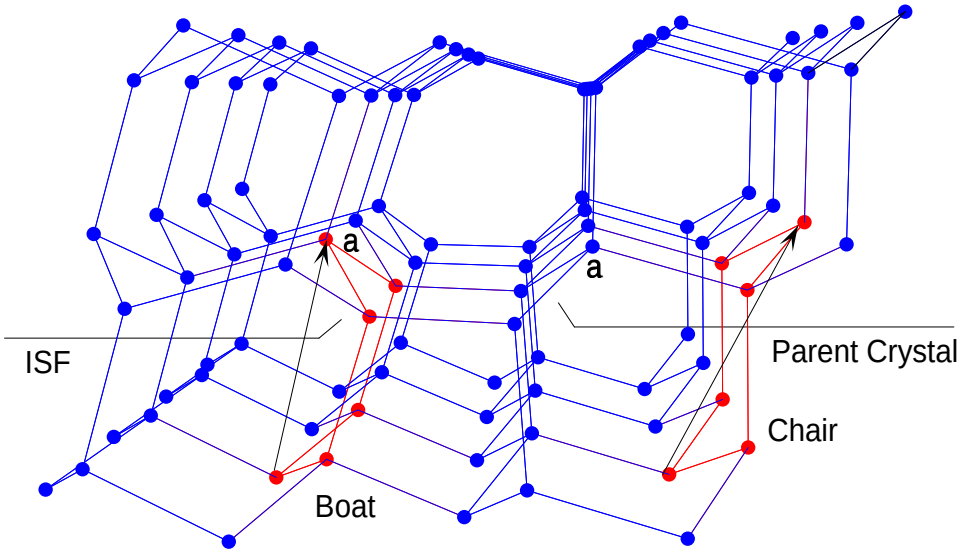

Figure 5

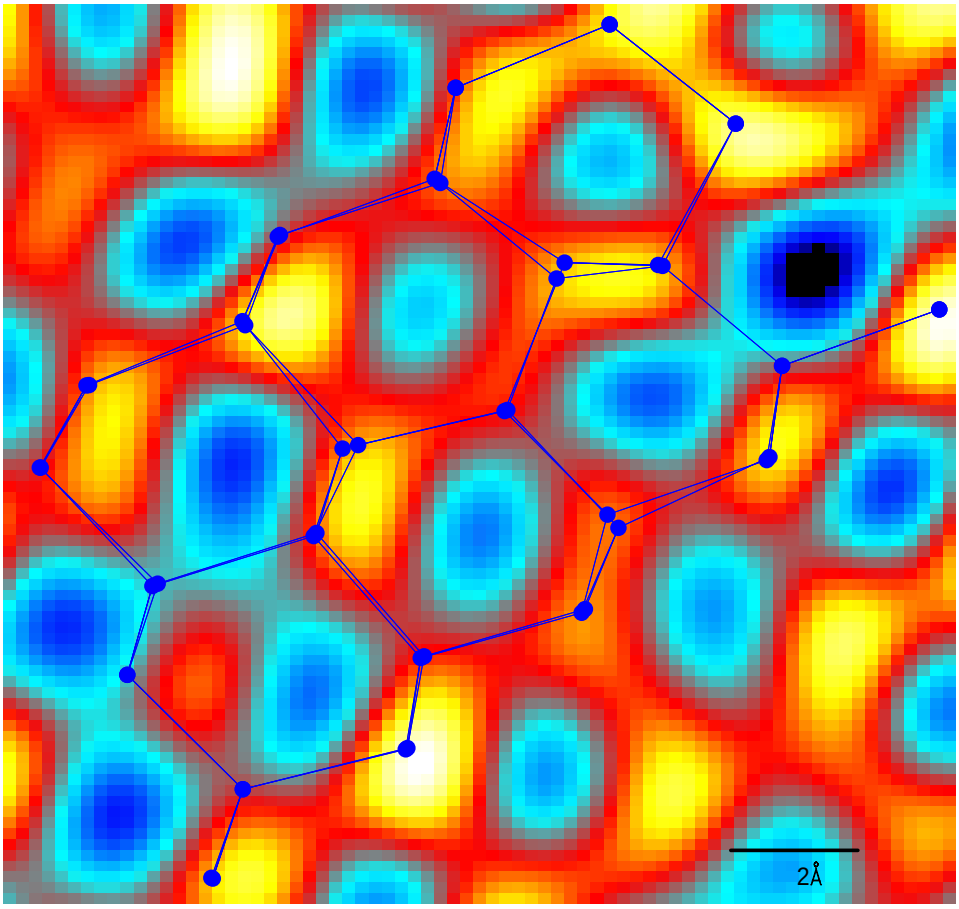

Figure 6

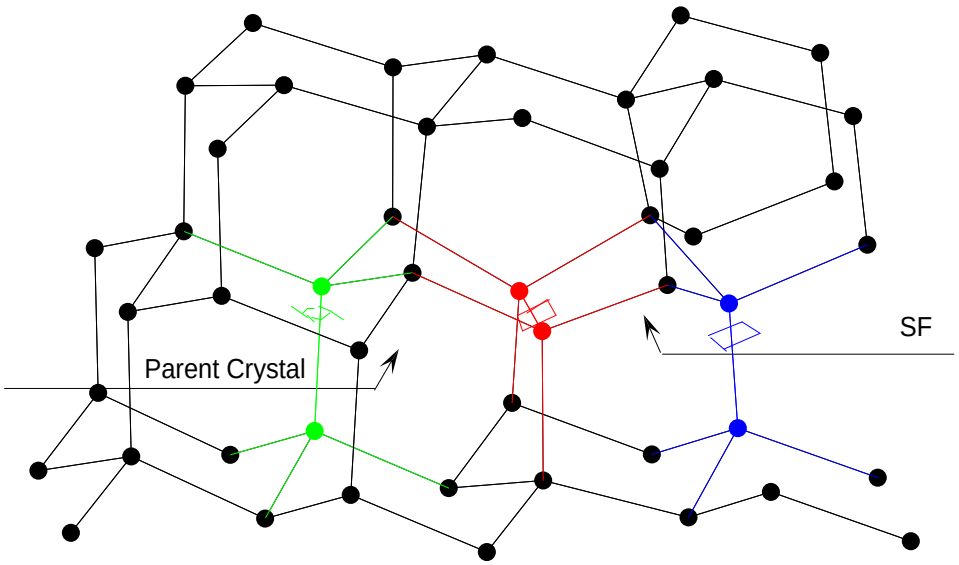

Figure 7

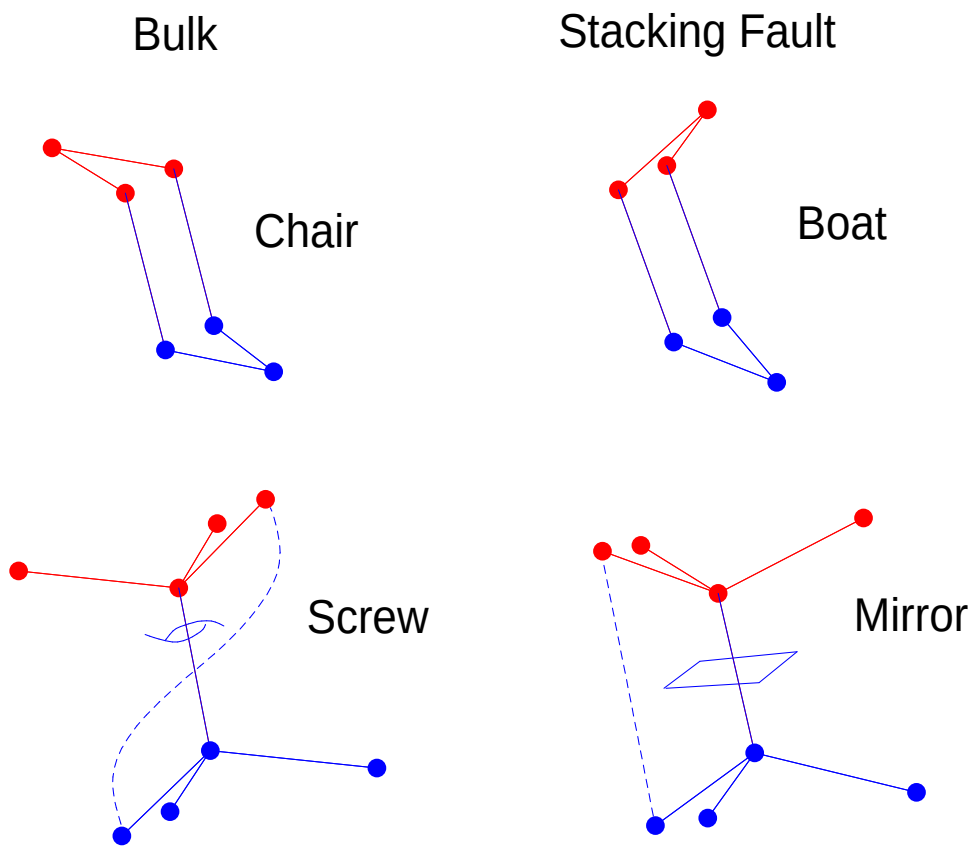

Figure 8

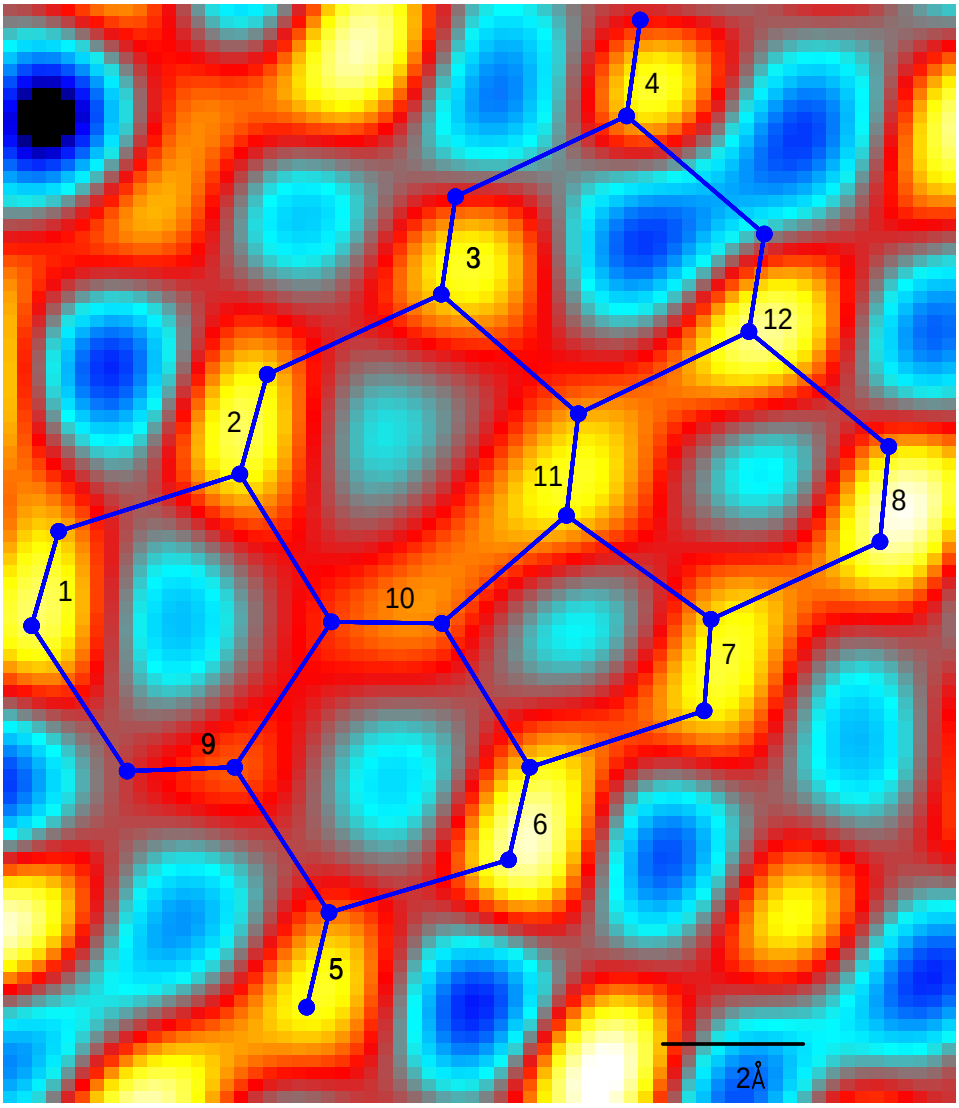

Figure 9

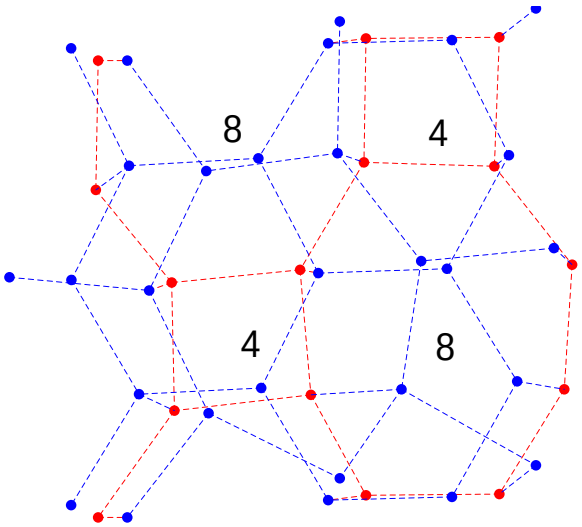

[1 1 1] Projection

[0 1 –1] Projection

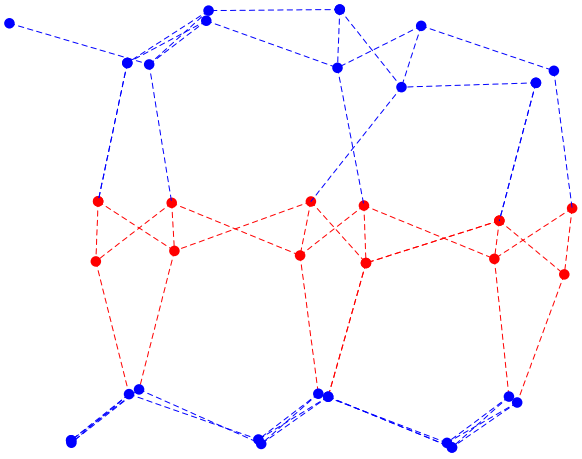

Figure 10

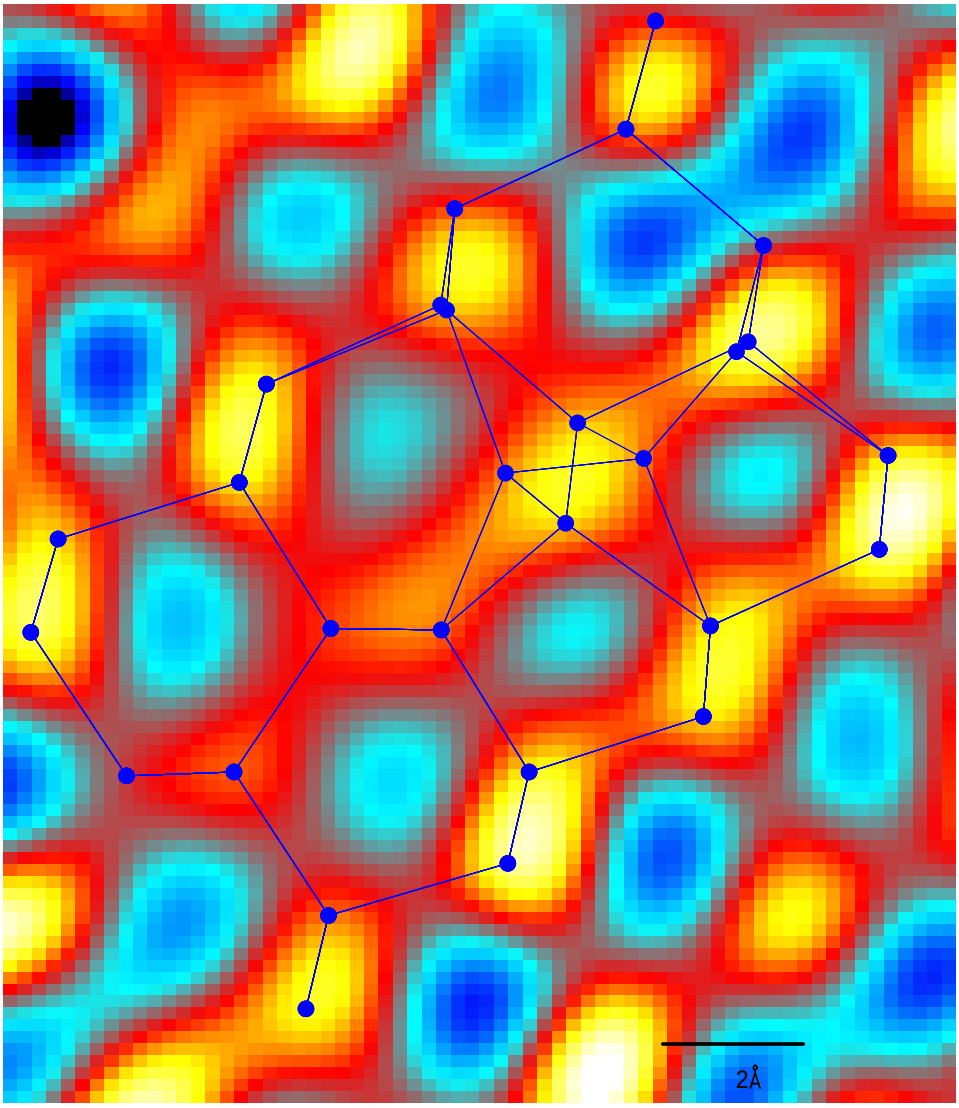

Figure 11

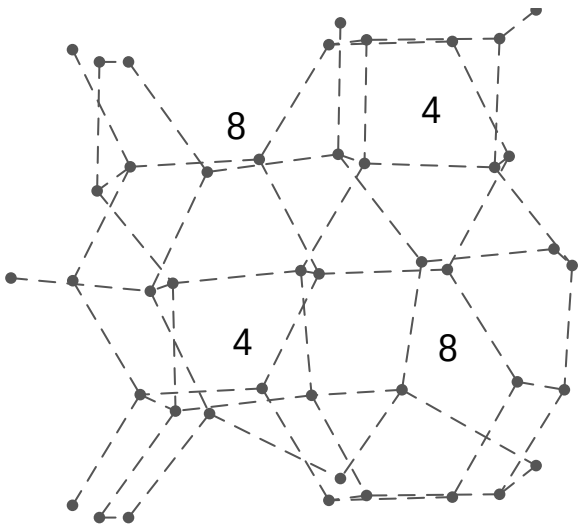

[1 1 1] Projection

[1 –1 1] Projection

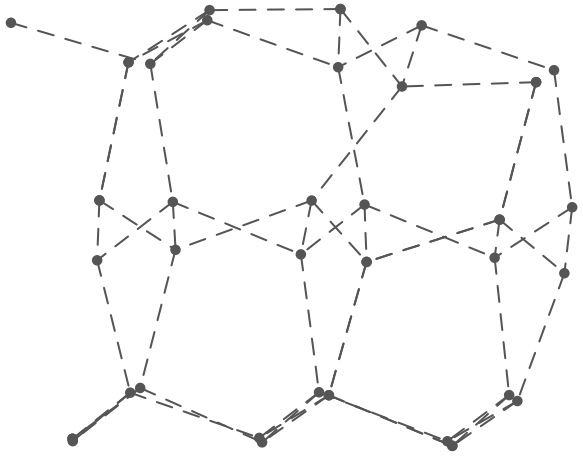

Figure 12

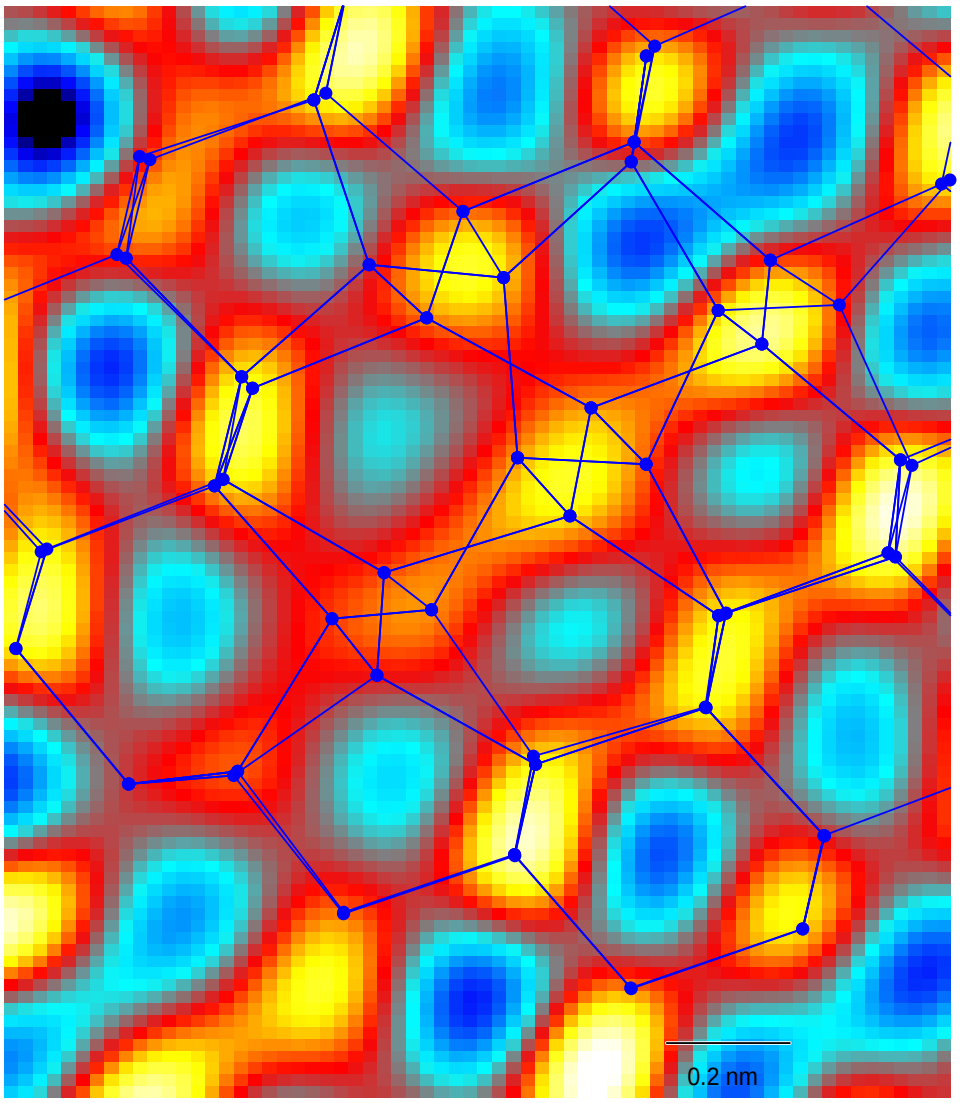

Figure 13

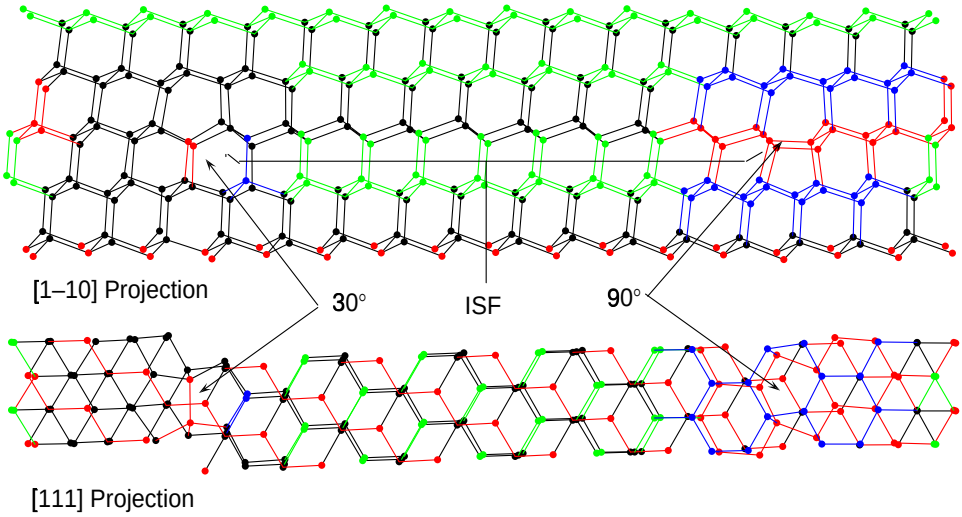

Figure 14

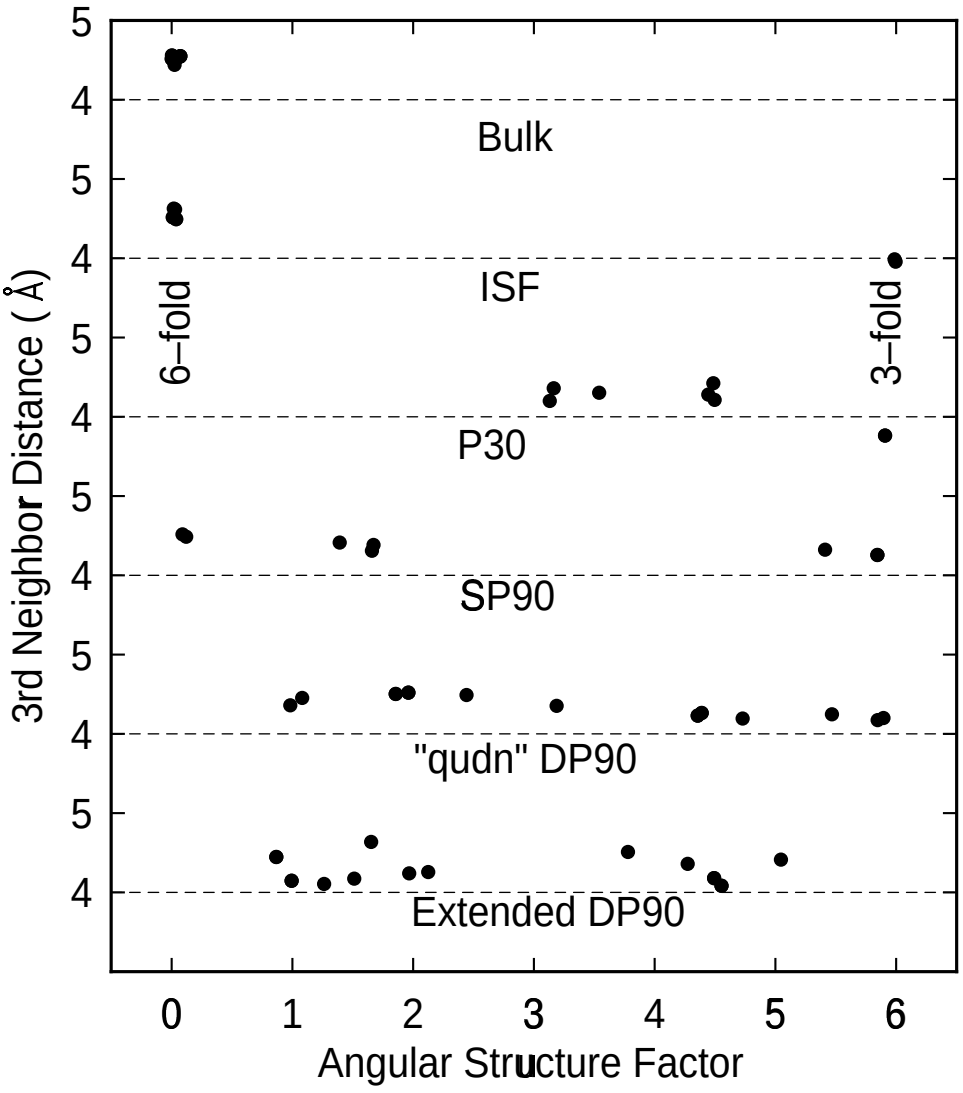
3rd Neighbor Distance (Å)
Angular Structure Factor
Bulk
ISF
P30
SP90
"qudn" DP90
Extended DP90
6–fold
3–fold
5
4
5
4
5
4
5
4
5
4
5
4
0
1
2
3
4
5
6

Figure 15

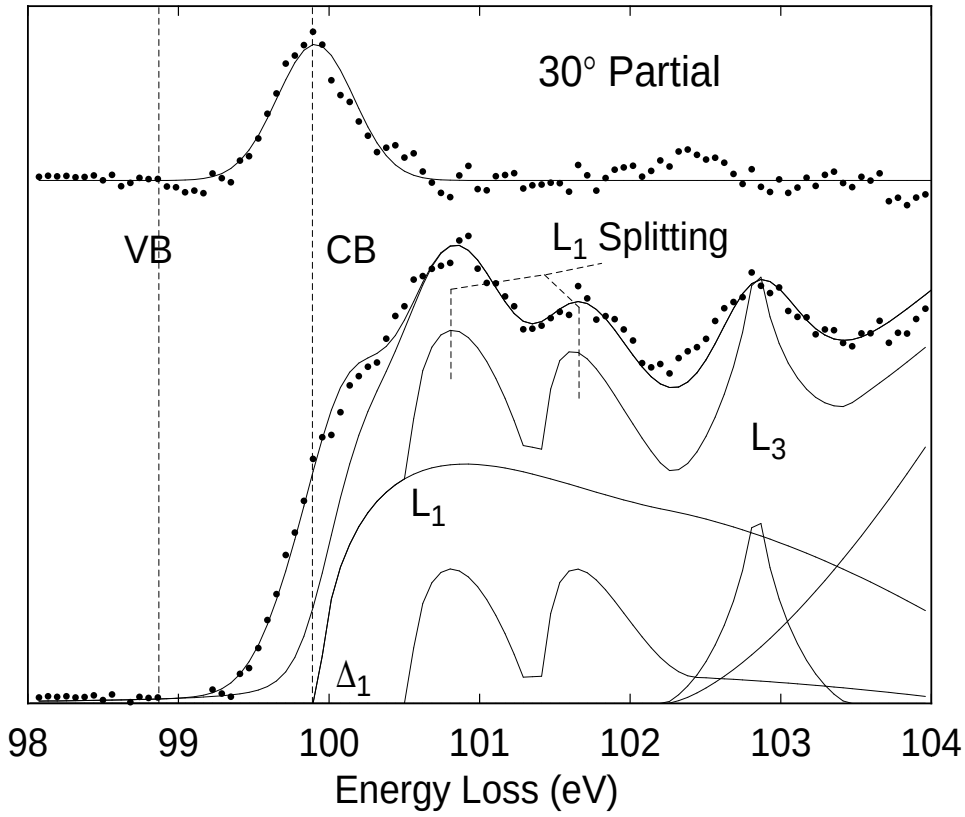
30° Partial
VB
CB
L1 Splitting
L3
L1
Δ1
98
99
100
101
102
103
104
Energy Loss (eV)

Figure 16

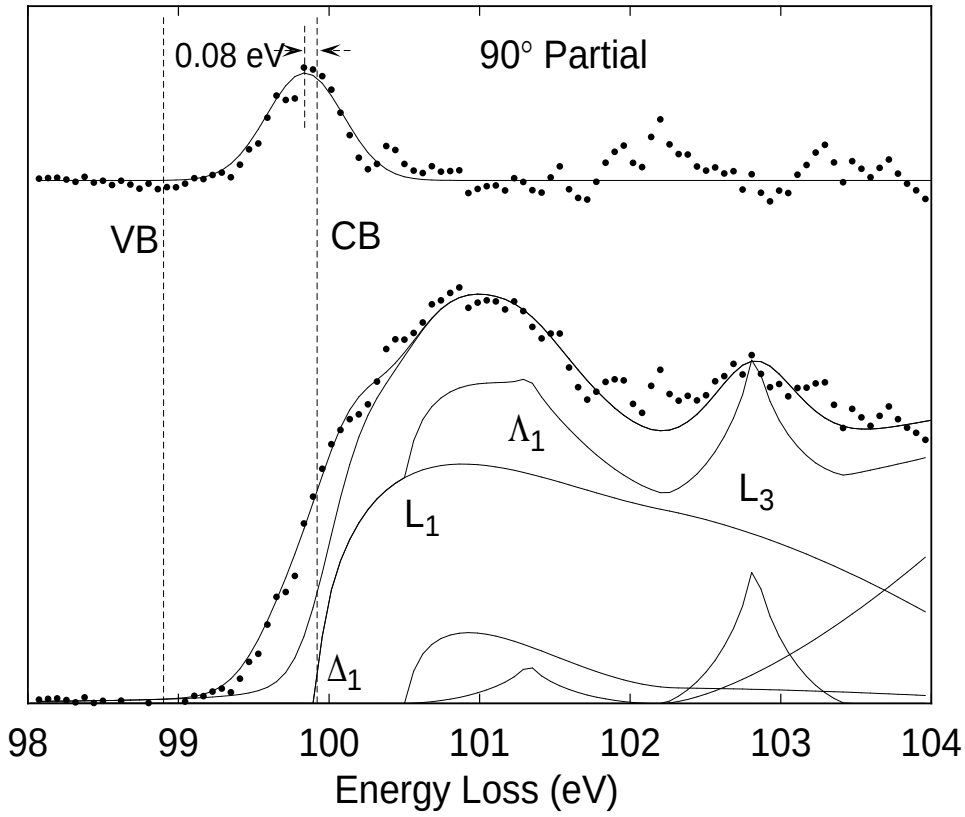
0.08 eV
90° Partial
VB
CB
Λ_1
L_3
L_1
Δ_1
98
99
100
101
102
103
104
Energy Loss (eV)

Figure 17